Available online at www.sciencedirect.com
ScienceDirect
Journal of Power Sources 174 (2007) 1224–1228
JOURNAL OF POWER SOURCES
www.elsevier.com/locate/jpowsour

Short communication

New Sn-based composites as anode materials for Li-ion batteries

A. Aboulaich [a,*], M. Mouyane [a], F. Robert [a], P.-E. Lippens [a], J. Olivier-Fourcade [a], P. Willmann [b], J.-C. Jumas [a]

[a] *Laboratoire des Agrégats Moléculaires et Matériaux Inorganiques (CNRS UMR 5072), Université Montpellier II, CC 015, Place E. Bataillon, 34095 Montpellier Cedex 5, France*
[b] *Centre National d'Études Spatiales, 18 avenue Edouard Belin, 31401 Toulouse Cedex 9, France*

Available online 30 June 2007

Abstract

A new strategy was developed to synthesize tin-composite materials. The Sn:BPO_4 and Sn:$CaSiO_3$ composites were obtained by solid state reaction, but the BPO_4 and $CaSiO_3$ matrices were synthesized by solid state reaction and sol–gel method, respectively. These materials are characterized by X-ray diffraction, ^{119}Sn Mössbauer spectroscopy and electrochemical tests. The results show that these new materials are efficient during electrochemical cycling (500 mAh g^{-1}), because of a good dispersion of Sn particles into the matrix. From the second cycle, charge and discharge reversibility is linked to both reversible Li_XSn alloy forming and the modification of the tin particle surface showed by Conversion Electron Mössbauer spectroscopy (CEMS) which allows us to characterize the sample surface. The irreversible capacity observed for the first charge/discharge cycle is due to tin oxide reduction and passivation of the anode surface by electrolyte solution decomposition (SEI layer).

Keywords: Sn-based composites; Lithium-ion batteries; Conversion Electron Mössbauer Spectroscopy; Anode materials; Tin based glass

1. Introduction

The increasing demand for high energy storage systems for new applications has driven extensive research on new Li-storage materials with improved electrochemical performances (high capacity, good cyclability and high level of safety). Over the last 15 years, many Li-alloy materials have been studied as possible anode materials for Li-ion batteries, because these materials show higher specific capacity than those obtained with the currently used carbon. Among these materials, Sn drew considerable attention because of two advantages, i.e. Sn has good electronic conductivity and a high theoretical specific capacity (993 mAh g^{-1}), corresponding to the formation of the lithium-richest alloy: $Li_{22}Sn_5$ (4.4 Li per Sn atom). However, this promising material shows poor cycling stability, due to significant volume changes between pure and fully lithiated tin (300%) which leads to the loss of electronic and mechanical contact. In order to solve this problem, Tin can be dispersed in a matrix to buffer volume changes, which makes it possible to maintain the electric contact within the anode materials.

Tin-based composite oxides developed by Fuji Photo Film ($SnB_{0.56}P_{0.4}Al_{0.42}O_{3.46}$) have drawn considerable attention [1]. The mechanism consists in reducing tin oxide into metallic tin which is dispersed *in situ* in an oxide matrix [2]. More recently, tin oxide and amorphous or crystalline boron phosphate ($Sn_2P_2O_7$, $Sn_3(PO_4)_2$, Sn_2BPO_6 and SnP_2O_7) were investigated [3,4]. The most noticeable deficiencies of Tin Composite Oxide are their irreversible capacity loss in the first charge cycle and their poor cyclability compared to carbon-based anodes.

Another method proposed in this study is to disperse the active species *ex situ* into an electrochemically inactive matrix. The purpose of dispersion is to improve the electrochemical performances, avoid pulverisation and reduce the stress in electrode materials [5,6].

This work focuses on the dispersion of the active tin species into two matrices, i.e. BPO_4 and $CaSiO_3$. The matrices were chosen because of their good thermal and electrochemical stability and good ionic conductivity [7,8].

The purpose of our work was to test the capacity of the BPO_4 and $CaSiO_3$ matrices in order to restrain the particle growth of the active phase during electrochemical tests.

The structural properties of these materials are characterized by X-Ray diffraction. In order to obtain an accurate analysis of the electronic structure of materials, we used ^{119}Sn

* Corresponding author. Tel.: +33 4 67 14 45 48; fax: +33 4 67 14 33 04.
E-mail address: abdelmaula.aboulaich@univ-montp2.fr (A. Aboulaich).

0378-7753/$ – see front matter © 2007 Published by Elsevier B.V.
doi:10.1016/j.jpowsour.2007.06.173

Mössbauer spectroscopy, in transmission (TMS) and emission modes (CEMS), which allows us to characterize crystalline and amorphous compounds.

The electrochemical performances were examined using a Swagelock^{TM} cell in galvanostatic mode.

2. Experiments

The BPO_4 and $CaSiO_3$ pristine materials were synthesized by solid-state route and sol–gel method, respectively. For solid-state reaction, the starting materials – H_3BO_4 and $NH_4H_2PO_4$ – were mixed in appropriate quantities so as to form a 2 g sample. The ground mixtures were homogeneously mixed using deionized water, and then heated in silica crucible at 180 °C in order to remove the volatile components and heated at 500 °C for different durations in a furnace [9].

The calcia-silicate powders were prepared by sol–gel method as previously described [10]. Tetraethyl orthosilicate TEOS and tetra hydrated calcium nitrate ($Ca(NO_3)_2{\cdot}4H_2O$) were used as precursors of SiO_2 and CaO, nitric acid was used as a catalyst and ethanol as a solvent. Briefly, a certain amount of TEOS was added to water under continuous stirring. The second solution was prepared with $Ca(NO_3)_2{\cdot}4H_2O$ in deionised water and added to the first solution and stirred for 2 h. The obtained solution was maintained at 60 °C until gelation occurred. The gel was dried at 80 °C and calcined at 730 °C for 4 h.

After optimizing both the structure and texture of the dispersion matrix, stoichiometric amounts of Sn (Aldrich, diameter <10 μm) and BPO_4 or $CaSiO_3$ were ground and heated in a vitreous carbon heating boat inside a horizontal tube furnace at 500 and 850 °C, respectively. This mixture was heated for 7 h in a constant flow of inert gas (nitrogen or helium) and cooled down to room temperature by quenching, after removing the boat from the furnace. The solid obtained gives a grey powder after grinding in agate mortar.

X-ray diffraction (XRD) measurements were carried out over the 2θ ranges from 10° to 90° with a Philips diffractometer using Cu Kα radiation (λ = 1.5418 Å).

^{119}Sn Mössbauer spectra were recorded in transmission geometry (TMS) in the constant acceleration mode using components manufactured by ORTEC and WISSEL. Conversion Electron Mössbauer Spectroscopy (CEMS) measurements were carried out using both a standard Mössbauer spectrometer with a constant acceleration movement and a gas flow (94% He, 6% methane) proportional counter to detect the internal conversion electrons emitted after resonant absorption of gamma rays. The source was ^{119m}Sn in a $CaSnO_3$ matrix and all spectra were collected at room temperature.

Electrochemical tests were carried out using a Swagelok^{TM} cell which contains a lithium foil as counter electrode. The working electrode was made by mixing active materials, acetylene black as the conductive agent, and polyvinylidene fluoride (PVDF) as the binder. The weight ratio of active powder, conductive agent and binder is 80:10:10. A solution containing 50 vol% ethylene carbonate (EC), 50 vol% dimethyl carbonate (DMC) and 1 M LiPF6 was used as the electrolyte solution and a Whatman paper (glass microfiber filters) was used as the separator. The cell was assembled in an Ar-filled glove box. The discharge–charge tests were carried out with a Mac Pile system operating in galvanostatic mode, in a constant current density between 1.2 and 0.1 V versus Li^+/Li^0.

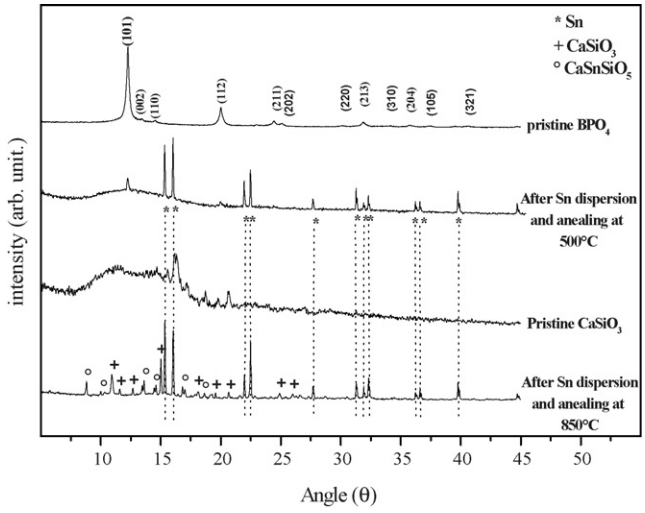

Fig. 1. XRD patterns of pristine materials (BPO_4 and $CaSiO_3$) and composite materials after Sn dispersion.

3. Results and discussion

The XRD patterns of the starting materials (BPO_4 and $CaSiO_3$ matrices) and the composites after dispersion of Sn are shown in Fig. 1. BPO_4 synthesized by solid-state reaction shows high crystallinity and it can be indexed in a tetragonal unit cell, space group $I4$. The following lattice parameters: $a = 4.338$ Å, $b = 4.322$ Å, $c = 6.635$ Å match the JCPDS file well (No. 79-1467).

After dispersion of tin powder, we observed a partial amorphisation of the matrix materials, a decrease in the intensity of the peaks, and the appearance of crystalline β-Sn which crystallizes in the tetragonal system, with the following lattice parameters $a = 5.827$ Å and $c = 3.181$ Å corresponding to the values found in the literature.

The X-ray patterns also show a broad scattering between 10° and 18°, probably due to the formation of an amorphous phase between the matrix materials and the active species dispersed. Mössbauer spectroscopy makes it possible to obtain more information and to characterize this phase more precisely.

For $CaSiO_3$ synthesized by sol–gel route, the gel-based material is obtained after heat treatment at 730 °C which is necessary to remove nitrate and residual organic groups. The presence of a diffusion "halo" is a feature of amorphous materials which do not show long-range order in the pristine sample.

After dispersion of tin particles within the matrix, the diffraction intensity increases, and typical β-Sn and $CaSnOSiO_4$ peaks appear. In addition, crystallization of $CaSiO_3$ is found in the powder.

The local electronic structure of Sn atoms has been characterized using ^{119}Sn TMS and CEMS in order to probe the bulk as well as the surface of these materials. The values of the hyper-

Table 1
Hyperfine parameters obtained from ^{119}Sn Mössbauer spectra shown in Fig. 2

Mössbauer mode	Tin sites	Sn:BPO_4				Sn:$CaSiO_3$			
		δ (mm/s)	Δ (mm/s)	Abs %	RC %	δ (mm/s)	Δ (mm/s)	Abs %	RC %
TMS	Sn^0	2.46 (13)	–	54	92	2.54 (13)	–	56	93
	Sn^{II}	3.45 (5)	1.45 (6)	46	8	2.93 (3)	1.89 (4)	14	2
	Sn^{IV}	–	–	–	–	−0.05 (5)	1.41 (4)	30	5
CEMS	Sn^0	2.34 (8)	–	17	67	2.58 (4)	–	26	78
	Sn^{II}	3.38 (5)	1.54 (6)	83	33	2.95 (5)	2.0 (10)	21	6
	Sn^{IV}	–	–	–	–	−0.03 (5)	1.41 (5)	53	16

The different types of tin used in the Mössbauer fitting procedure and their relative contributions in the total absorption (Abs) in the Mössbauer spectra, the values of the isomer shift δ, the quadrupole splitting Δ and the relative concentration (RC) calculated using the following values of the Lamb-Mössbauer factor f: $f(Sn^{II}) = f(Sn^{IV}) = 0.4$, $f(Sn^0) = 0.04$

fine parameters obtained from TMS and CEMS spectra recorded at room temperature are included in Table 1. Two components are observed for the Sn:BPO_4 composite in TMS (Fig. 1a′), Sn^{II} fitted with a quadrupole doublet, with the following hyperfine parameters; isomer shift (I.S.) $\delta = 3.45$ mm s and quadrupole splitting (Q.S.) $\Delta = 1.45$ mm s. The other component is fitted with a singlet due to the contribution of Sn^0 with a $\delta = 2.37$ mm s isomer shift. The contribution of these species (Abs) to the total absorption area depends on the Lamb-Mössbauer factor f values of each tin site. That is why the relative concentration (RC) of tin in the different species can be deduced from the corresponding (Abs) areas only if the f values are known. The values of the hyperfine parameters of Sn^{II} are similar to those observed for the $SnB_{0.6}P_{0.4}O_{2.9}$ glass which was studied by Chouvin et al. [11], so we used as the f factor the following values: 0.4 for Sn^{II} [12], 0.04 for Sn^0 [13], and 0.4 for Sn^{IV} [14]. Therefore, the real concentration in bulk is 92% for Sn^0 and only 8% for Sn^{II}.

In Emission mode (Fig. 2a′), we found the same components but the surface area of the Sn^{II} signal (83%) is higher than that of Sn^0 (17%). The relative concentration of Sn^{II} on the surface (33%) is higher compared with those in the bulk.

For the Sn:$CaSiO_3$ composite, the Mössbauer absorption spectra are shown in Fig. 2b. The spectra can be interpreted considering three main components whose contributions values are evaluated by taking into account the Lamb-Mössbauer factors listed in Table 1.

In TMS, the real contribution of Sn^0 due to the β-Sn particles is higher (93%) compared with the two other contributions. In emission mode we observe no difference between the hyperfine parameters of the different components, but we note an increase in the contribution of Sn^{II} and Sn^{IV} as compared to that of Sn^0. So, Sn^{IV} tends to form more on the surface of $CaSiO_3$. This component with a high quadrupole splitting ($\Delta = 1.41$ mm s) is due to the formation of crystalline $CaSnOSiO_4$ as shown in X-ray patterns.

In Table 2, we summarize the evolution of the composition on the surface and in the bulk of the different compounds. We observe that the percentage of amorphous tin(II) increases on the surface in the case of the Sn:BPO_4 materials, even though the percentage of Sn^0 decreases.

For Sn:$CaSiO_3$, the amount of $CaSnSiO_5$ on the surface increases compared with those in the bulk, even though the quantity of Sn^{II} remains quite stable.

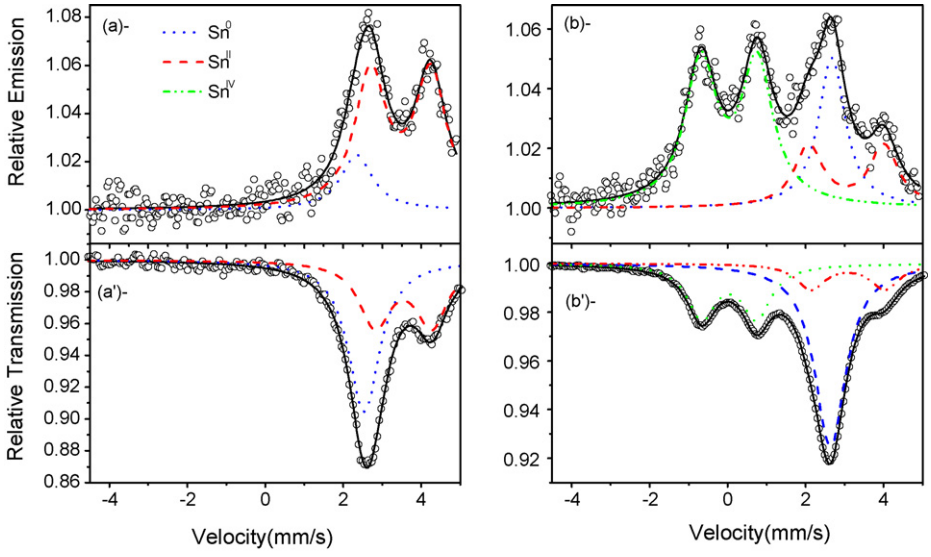

Fig. 2. ^{119}Sn Mössbauer spectroscopy spectrum for Sn:BPO_4 (a and a′) and Sn:$CaSiO_3$ (b and b′) in transmission and emission mode.

Table 2
Summary of the bulk and the surface composition studied by XRD and ^{119}Sn Mössbauer spectroscopy, ↗ (increase); ↘ (decrease)

$Sn:BPO_4$		$Sn:CaSiO_3$	
Bulk	Surface	Bulk	Surface
XRD			
BPO_4	–	CaSiO3	–
β-Sn		β-Sn	
Amorphous phase		$CaSnSiO_5$	
Mössbauer			
Amorphous Sn^{II}	Amorphous Sn^{II} ↗	Amorphous Sn^{II}	Amorphous Sn^{II}
β-Sn	β-Sn ↘	β-Sn	β-Sn ↘
		$CaSnSiO_5$	$CaSnSiO_5$ ↗

Discharge and charge performances of these electrode materials were tested via Swagelok™ cell using a Mac pile in galvanostatic mode. Fig. 3 shows the first two cycles of the $Sn:BPO_4$ and $Sn:CaSiO_3$ anode materials tested at *C*/20 and *C*/10 rate, in potential windows [0.1–1.2 V] and [0.01–1.2 V], respectively.

The small plateau at 1.5 V is due to the reduction of Sn^{II} which leads to the formation of an amorphous interface between the Sn^0 particles and the borophosphate matrix. At 0.8 V, the small shoulder is associated to the formation of the first Li–Sn alloy (Li_2Sn_5), we observe a large plateau at 0.58 V corresponding to a LiSn alloy formation. Between 0.4 and 0.1 V, the absence of plateau for Li_7Sn_3, Li_5Sn_2 and $Li_{13}Sn_5$ during Li is caused by the relatively identical enthalpy of formation of these alloys.

Nearly similar potential profiles are also seen in the case of the $Sn:CaSiO_3$ composite. However, two differences are observed. The first one is the absence of plateau at 1.57 V associated to a Sn^{II} reduction because of the small quantity of Sn^{II}. This plateau is replaced by a small one at around 0.89 V due to the Sn^{IV} reduction into Sn^0. The second one is the absence of plateau at 0.58 V because the cell is cycled at fast rate (*C*/10). Therefore, Sn^{II} and Sn^{IV} have hardly any influence on the electrochemical potential curve of the $Sn:CaSiO_3$ composite.

During the first charge, the electrochemical behaviour is similar for both materials, therefore we show better reversibility for the $Sn:CaSiO_3$ composite compared to $Sn:BPO_4$. In the second discharge, same plateaus are observed for the two materials.

During charge–discharge processes, the polarization is lower compared with pure nanosize Sn. This can be explained by both a good electric contact of the electrode material and a decrease in volume expansion contraction during Lithium insertion/extraction. The matrix can buffer volume changes and avoid the impact of the shrinkage of actives particles on electric conductivity.

Fig. 4 shows the discharge capacity of the $Sn:BPO_4$ and $Sn:CaSiO_3$ composites cycled at *C*/20 and *C*/10 rates, respectively. During the first cycle, irreversible capacity around 200 mAh g^{-1} is observed. This irreversible part may be linked to both the formation of a passivation film one the electrode surface because of the electrolyte degradation at the electrode/electrolyte interface and to the reduction of Sn^{II} forming the interface in the $Sn:BPO_4$ composite and/or to the reduction of Sn^{IV} for the $Sn:CaSiO_3$ composite. The reversible capacity is high for both materials (500 mAh g^{-1}) and capacity retention is higher than 98% after the eighth cycle.

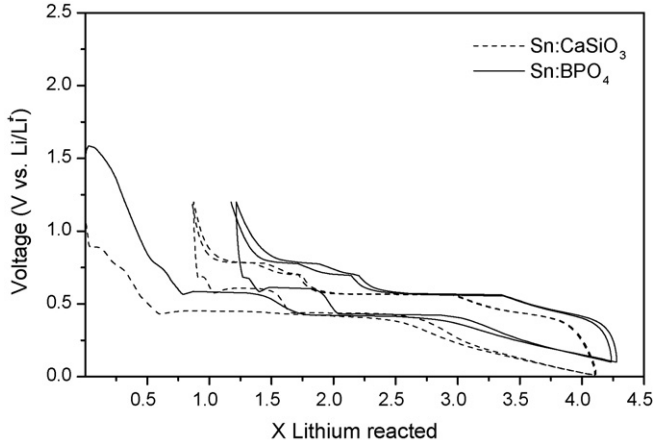

Fig. 3. First two discharge charge curves obtained for $Sn:BPO_4$ and $Sn:CaSiO_3$ composites at *C*/20 and *C*/10 rates, respectively.

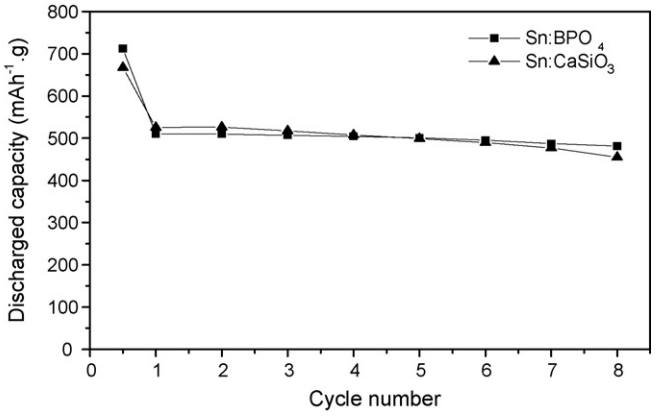

Fig. 4. Discharge capacity vs. number of cycle for $Sn:BPO_4$ and $Sn:CaSiO_3$ composites.

4. Conclusion

Dispersion of tin particles in a crystalline borophosphate matrix allows the pinning of these particles in the matrix by an amorphous Sn^{II} boron phosphate glass interface. In an amorphous calcia-silicate matrix, a new crystalline component is formed at the interface ($CaSnSiO_5$), observed by XRD and Mössbauer spectroscopy. Both Crystalline $CaSnSiO_5$ and amorphous Sn^{II} are responsible for the good retention capacity during the alloying/desalloying reactions.

These new Sn-based composite materials show good cyclability and high discharge capacity as compared to carbon. The performances are due to either an amorphous (boron phosphate matrix) or crystalline (calcium silicate matrix) interface formed between active/inactive materials. Pinning makes it possible to maintain the metallic tin performances, while absorbing volume change and avoiding particle coalescence.

The active/inactive material ratio is essential to obtain good electrochemical performances. Our future research projects will focus on the optimization of this parameter.

Acknowledgements

The authors acknowledge European network of excellence ALISTORE (contract no. SES6-CT-2003-503532), Centre National d'Etudes Spaciales (Toulouse, France) (contract no. 04/1756/00) and SAFT Bordeaux (contract no. 752295/00) for the financial support.

References

[1] Y. Idota, T. Kubota, A. Matsufuji, Y. Maekawa, T. Miyasaka, Science 276 (1997) 1395.
[2] I.A. Courtney, J.R. Dahn, J. Electrochem. Soc. 144 (1997) 2045.
[3] M. Behm, J.T.S. Irvine, Electrochim. Acta 47 (2002) 1727–1738.
[4] J.Y. Lee, Y. Xiao, Z. Liu, Solid State Ionics 133 (2000) 25–35.
[5] J.-C. Jumas, F. Robert, P.E. Lippens, J. Olivier-Fourcade, P. Willman, Patent no. FR2873855 (2004).
[6] A. Aboulaich, L. Aldon, F. Robert, P.E. Lippens, J. Olivier-Fourcade, P. Willmann, Jean-Claude Jumas, Hyp. Interact. 167 (2006) 733–738.
[7] E.M. Kelder, M.J.G. Jak, F. De Lange, J. Schoonman, Solid State Ionics 85 (1996) 285–291.
[8] M. Malki, P. Echegut, J. Non-Cryst. Solids 323 (2003) 131.
[9] J. Haines, C. Château, J.M. Leger, R. Marchand, Ann. Chim. Sci. Mater. 26 (2001) 209–216.
[10] P. Saravanapavan, L.L. Hench, J. Non-Cryst. Solids 318 (2003) 1–13.
[11] J. Chouvin, C. Branci, J. Sarradin, J. Olivier-Fourcade, J.-C. Jumas, B. Simon, Ph. Biensan, J. Power Sources 81–82 (1999) 277.
[12] F. Robert, P.E. Lippens, J. Olivier-Fourcade, J.-C. Jumas, M. Morcrette, J. Power Sources 146 (2005) 492–495.
[13] A.A. Bakgat, Phys. Status Solidi B 97 (1980) K129.
[14] M.S. Moreno, R.C. Mercador, Phys. Rev. B (1994) 9875.